Dependence upon charge of the vibrational spectra of small Polycyclic Aromatic Hydrocarbon clusters: the example of pyrene

Léo Dontot, Fernand Spiegelman, Sébastien Zamith, Mathias Rapacioli

EPJ manuscript No.
(will be inserted by the editor)

Dependence upon charge of the vibrational spectra of small Polycyclic Aromatic Hydrocarbon clusters : the example of pyrene

Léo Dontot[1], Fernand Spiegelman[1], Sébastien Zamith[2] and Mathias Rapacioli[1]

[1] Laboratoire de Chimie et Physique Quantique (LCPQ/IRSAMC), UMR5626, Université de Toulouse (UPS) and CNRS, 118 Route de Narbonne, F-31062 Toulouse, France
[2] Laboratoire Collisions Agrégats Réactivité (LCAR/IRSAMC), UMR5589, Université de Toulouse (UPS) and CNRS, 118 Route de Narbonne, F-31062 Toulouse, France

the date of receipt and acceptance should be inserted later

Abstract. Infrared spectra are computed for neutral and cationic clusters of Polycyclic Aromatic Hydrocarbon clusters, namely $(C_{16}H_{10})_{n=1,4}^{(0/+)}$, using the Density Functional based Tight Binding scheme combined with a Configuration Interaction scheme (DFTB-CI) in the double harmonic approximation. Cross-comparison is carried out with DFT and simple DFTB. Similarly to the monomer cation, the IR spectra of cluster cations are characterized by a depletion of the intensity of the CH stretch modes around 3000 cm^{-1}, with a weak revival for $n = 3$ and 4. The in-plane CCC modes in the region 1400-2000 cm^{-1} are enhanced while the CH bending modes in the range 700-1000 cm^{-1} are significantly weakened with respect to the monomer cation, in particular for $n = 2$. Finally, soft modes corresponding to diedral fluctuations of the monomers within the central stack of the ion structure, possibly mixed with monomer folding, are also observed in the region 70-120 cm^{-1}.

PACS. XX.XX.XX No PACS code given

1 Introduction

Clusters of Polycyclic Aromatic Hydrocarbons (PAHs) have been the subject of various experimental and theoretical investigations over the past decades due to their interest in several research fields. For instance, their role in flame chemistry is still under debate, as they could act as possible precursors of soot particles through oligomerization[1–12]. The optical and transport properties of PAH clusters are also investigated in the context of organic solar cell design [12–21]. Carbonaceous compounds involving PAH are studied as pollutants in both environmental and atmospheric science [22–26]. In astrophysics, PAHs have been proposed in the mid-eighties as precursors of mid-infrared emission bands[27,28] as well as contributors to the Diffuse Interstellar Bands (DIBs), a series of UV-Visible absorption bands [29–32]. Observations made with the Infrared Space Observatory and the Spitzer Space Telescope suggested that free flying PAHs result from the evaporation of larger grains, possibly PAH clusters[33–35]. PAH clusters are also suspected to contribute to some of the DIBs and the extended red emission and to play a role in the growth of interstellar PAHs[16,36–39]. Not only there is a need for characterizing the spectral properties of neutral clusters, but also to address their dependence upon charge, as previously done for free-flying PAH molecules, either ionized or protonated [40–48].

A number of studies focused on the characterisation of the structural properties of PAH clusters, in particular discussing the appearance of stack patterns [9,49–59]. The structures of neutral clusters are governed by steric effects and long-range interactions. It is obviously necessary to use a methodology adequate to describe long range forces and in particular the dispersion forces. Unfortunately, highly accurate methods such as Coupled Cluster or MP4, fully relevant to deal with weakly bound closed shell molecular systems, are quite accurate if large basis sets are involved but computationally demanding and hence have not been used for PAH clusters larger than dimers. Their IR spectra have been investigated both experimentally and theoretically [59–61]. Ricca *et al.* gave a quite thorough IR theoretical harmonic characterization of various isomers of neutral pyrene clusters at the DFT+D3 level[59].

The theoretical investigation of cationic clusters is even more delicate. Indeed in addition to long range forces, the charge localization must me treated correctly. At the DFT level, traditional functionals undergo self-interaction artifacts leading to improper description of dissociated rad-

Correspondence to: mathias.rapacioli@irsamc.ups-tlse.fr

ical cations [62]. Several schemes have been developed to correct those artifacts, such as the long-range short-range schemes which allow to treat differently the short dynamical correlation and the long-range non-dynamical correlation[63–66]. Similar implementations have been done [67] with the context of Density Functional based Tight Binding (DFTB [68–71]), an approximation of DFT which is computationally more efficient than DFT and able to deal with larger systems. Other schemes can be used to avoid overdelocalization problems in charged molecular clusters. In the past decade, we have developed a model combining Configuration Interaction with the DFTB (hereafter labeled DFTB-CI) [72], which is an adaptation of the DFT-CI scheme [73] to the DFTB framework.

The coupling of DFTB and DFTB-CI with a global exploration scheme allowed us to obtain low energy structures for cationic and neutral pyrene clusters [74], providing binding energies and ionisation potentials in agreement with experimental measurements [75,76]. We report, in the present work, the IR spectra of cationic and neutral pyrene clusters, namely dimers, trimers and tetramers, obtained with DFTB-CI for cations and DFTB for neutrals. In particular, we address the IR spectra dependence upon size and charge. We also present comparison with first principle DFT spectra. In the next section, we briefly describe the scheme used to compute these spectra before presenting and discussing the results.

2 Method

The IR spectra presented for the most stable structures of pyrene clusters are computed here within the double harmonic approximation. Three electronic structure methods have been used to compute these spectra, namely DFTB for neutrals, DFTB and DFTB-CI for the ions and DFT for common reference calculations. The DFT calculations have been performed with the Gaussian09 [77] package using the B3LYP functional with D3 dispersion correction combined with the extended basis cc-pVDZ. We quickly summarize the essential ingredients of the DFTB scheme used here [68–71]. In its most common SCC (self-consistent-charge) formulation [70], DFTB is derived from DFT through a second order expansion of the DFT energy around a reference density, taken as the sum of isolated atomic densities. The neglect of three-center integrals allows for building the DFTB Kohn Sham operator from two-center pre-tabulated DFT data, Mulliken definition of the atomic charges and Hubbard atomic parameters. In the present work, we use the set of matsci-0-3 parameters [78] as well as the weighted Mulliken (Wmull) charge scheme [79,80], allowing for a better description of intermolecular coulomb interactions, and a dispersion correction scheme [50]. Note that the use of different charges also improves the dipole moments, a crucial quantity for the determination of IR spectra [81]. In the case of cationic clusters, we will also work in the framework of the configuration interaction DFTB-CI scheme [72] to properly describe the charge delocalization over different units. Briefly, the DFTB-CI scheme is implemented in a basis of valence-bond type configurations Φ^+_{Ak} obtained via DFTB with a constraint of charge localization on a given molecule of the cluster. The DFTB-CI energies are thus the eigenvalues of a non-orthogonal CI problem whose size is equal (k=HOMO only) or scales (k=HOMO,HOMO-1...) as the number of molecules, corresponding to ground state eigenvectors Ψ^+_0 incorporating charge delocalization as a combination over the charged localized configurations

$$\Psi^+_0 = \sum_{Ak} c^0_{Ak} \Phi^+_{Ak} \quad (1)$$

Note that, in the case of the cationic monomer, DFTB-CI is reduced to simple DFTB. The DFTB and DFTB-CI calculations have been carried out with the deMonNano package [82]. In the following and for sake of simplicity, we will generally refer to DFT, DFTB or DFTB-CI, the previously mentioned calculation details (+D/ +D3/ Wmull/ SCC) being implicit.

All presented spectra result from convolution of the lines originating from the diagonalisation of the weighted Hessian matrix with lorentzian functions with half-width 15 cm^{-1}.

3 Results

We start here with the monomer. The present subsection is not supposed to bring new information about the IR spectra of the pyrene monomer and its cation, abundantly documented in the literature but to measure the performance of DFTB as an approximate DFT method for the vibrational observables of this constituting molecule. The spectrum of neutral pyrene has been experimentally determined by a number of authors, either in cryogenic matrices[41,83] or in gas phase[86,83]. Joblin *et al.*[83] provided full range spectroscopy of pyrene in neon matrices at 4K, the lines with largest intensity occurring around peaks at 713, 844, 1087/1097, 1605 and 3053/3064 cm^{-1} while the gas phase experiments of Malteseva *et al.*[86] only concerned the range 3044-3118 cm^1. Essentially, the region 700-900 cm^{-1} corresponds to CH out of plane bending modes, that between 1000 and 1800 cm^{-1} to in-plane CCC or CH bending (possibly coupled) modes and the features around 3000 cm^{-1} to CH stretching modes. Some weaker intensity patterns are also observed in the region 1405-1430 cm^{-1}. A number of theoretical studies, either at the HF level[41] or at the DFT level[40,42], were devoted to the IR bands assignments. In most calculations, the double harmonic approximation was used, corrected by scaling factors. Mackie *et al.*[87] and Mulas *et al.*[88] have explored theoretically the importance of anharmonicities. The work of Mulas *et al.* is based on a DFT potential surface with the B97-1 hybrid functional, which provides, after applying a scaling factor, harmonic lines (largest intensities at 713, 845, 1089, 1606 and 3057/3074 cm^{-1}) in close correspondence with the experimental results. Anharmonicities are shown to induce small shifts of a few cm^{-1} depending on the spectral region. More significant

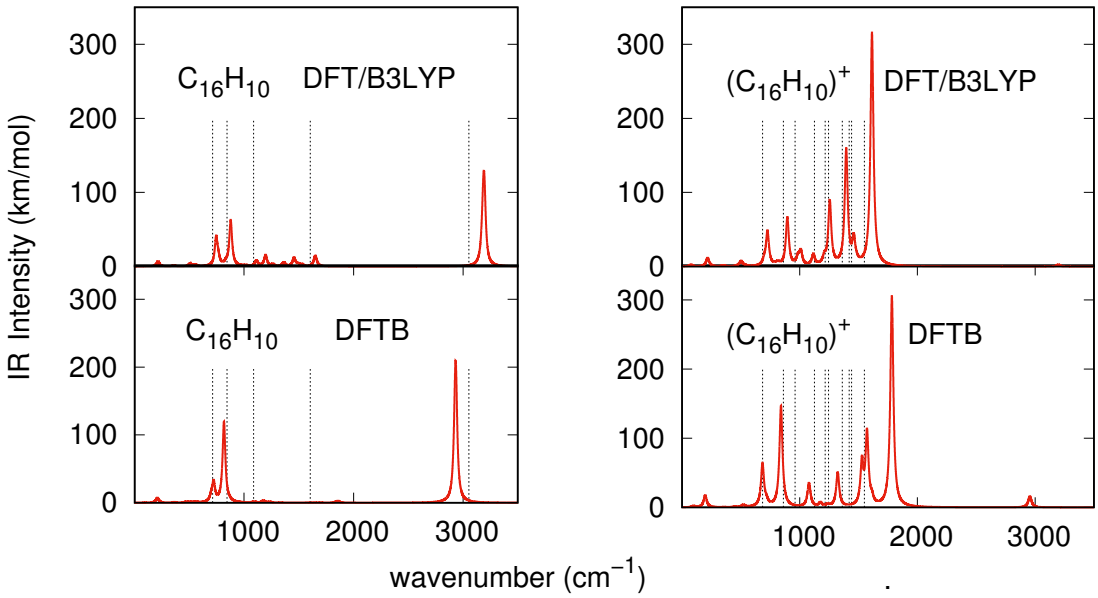

Fig. 1. Harmonic IR spectra of neutral and cationic pyrene monomer with DFT/B3LYP and DFTB. The vertical dashed lines indicate the experimental frequencies of the major intensity modes for neutral [83] and cationic [41,84,85] pyrene

changes are observed for the intensities, due to mode mixing. We will take as reference here standard DFT calculations achieved using the hybrid B3LYP functional, the most commonly used to calculate IR spectra. Despite DFT calculations already exist[40,42,88] for the monomer, we have repeated them here to have a global common benchmark with the same functional and the same basis set for monomers and small clusters, neutral and singly charged. It can be seen in figure 1 that DFT/B3LYP yields lines at 746, 878, 1112/1196, 1455, 1648 and 3186/3196 cm^{-1}. The DFTB results of the neutral monomer reproduce reasonably the DFT spectrum, with three peaks at 722, 816 and 2929 cm^{-1} and very weak bumps at 1175 and 1858 cm^{-1}. The relative errors on the DFT peaks *vs* the experimental values are in the range of 3 to 10 percent. Fortuitously, the errors of DFTB on the three main peaks *vs* the corresponding experimental values above are found to be below 5 percent. One can however observe that in the region 900-1700 cm^{-1} (in plane CCC stretching modes), the intensities of the DFTB bands almost completely vanish, while the DFT peaks remain small but still visible, more consistent with the experimental results[41,83]. Despite these differences, the qualitative assignment in DFT and DFTB is consistent. In the following, since we will be mostly interested in the changes induced by clustering effects, we will not apply any scaling factors.

The IR spectrum of the singly charged pyrene monomer has also been investigated experimentally either from absorption in argon matrices [41] or in gas phase via the Single Photon Infra Red emission technique[84,85] (SPIRES). The spectrum is strongly different from that of neutral pyrene with a vanishing intensity for the stretching CH modes around 3000 cm^{-1} and lines with significant intensities at 685, 862, 961, 1125, 1217, 1245, 1362/1459, 1420, 1441 and 1550 (the most intense). This large change was reported theoretically[41,40,42] and interpreted by Torii *et al.*[89]. In their interpretation the collective in-plane vibrational motion of the carbon atoms couples with strong fluctuations of the dipole moment over the molecule skeleton. This coupling induces significant charge fluxes which dominates the in-plane CH stretch intensity contributions to the spectrum. All together, these give rise to a much richer pattern in the 1000-2000 cm^{-1} region and vanishing intensity around 3000 cm^{-1} It can be seen in Figure 1 that these trends are correctly reproduced both at the DFT level, as previously reported[41,40], and DFTB level. The main DFT peaks are at 726, 895, 1256, 1395/1460 and 1613/1615 cm^{-1}. The main DFTB maxima point at 684, 841, 1323, 1529/1572 and 1781/1784 cm^{-1}. The analysis shows that the same types of modes are observed for the lines obtained at the DFT wavenumbers 726, 895, 1256 and 1613/1615 cm^{-1} and at the corresponding DFTB values at 684, 841, 1323 and 1781/1784 cm^{-1} respectively. The mixing of the analogous in-plane CCC and CH modes is however different for frequencies 1395/1460 in DFT cm^{-1} (1529/1572 in DFTB), due to de-

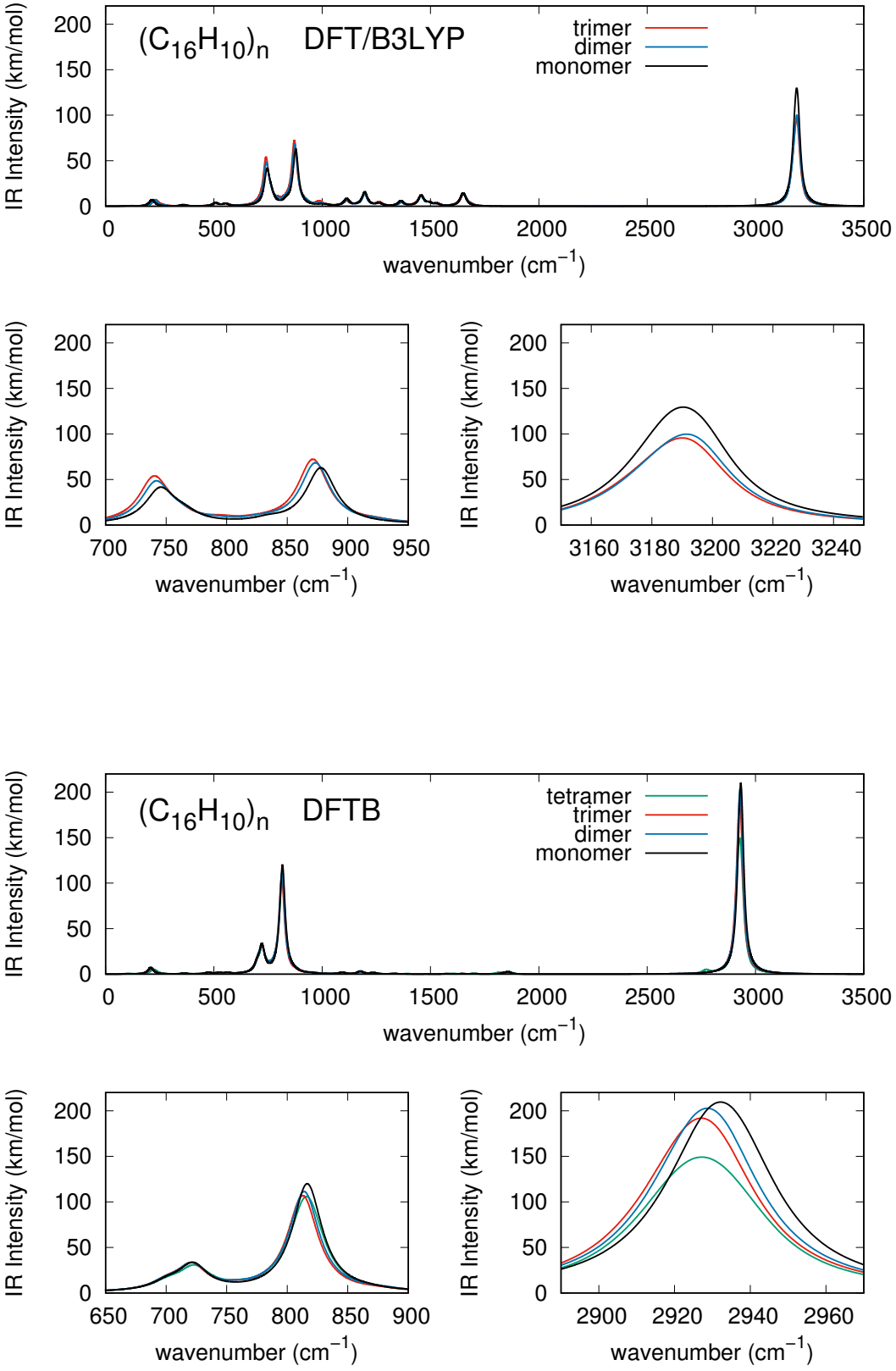

Fig. 2. Harmonic IR spectra of $(C_{16}H_{10})_{n=1,4}$ clusters from DFT/B3LYP (top) and DFTB (bottom) calculations. For each method, two zoom views in the 700-900 cm^{-1} range and around 3000 cm^{-1} regions, respectively, are shown below the full spectrum graph.

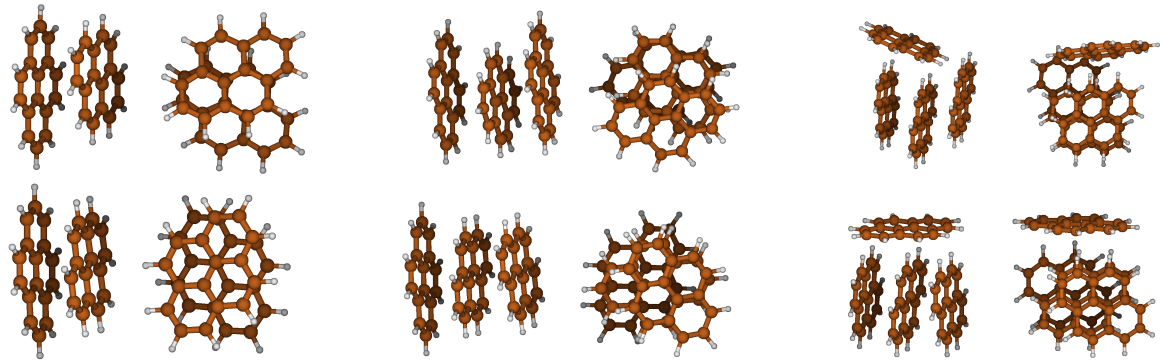

Fig. 3. Geometries of neutral (top) and cationic (bottom) pyrene clusters, n=1-4 from left to right. For each structure, side (left) and top (right) views

generacy. The largest intensity at 1613/1615 corresponds also to a mixing of in-plane CCC and CH modes. In the cation, the frequency relative errors of DFTB with respect to DFT remain below 10 percent. Comparing with experiment, the largest DFTB discrepancy (15 percent) is obtained for the band at 1781/1784 cm^{-1}.

We now comment results obtained for clusters. Crossed comparisons of the IR spectra computed at the various levels of theory are given for neutral and cationic pyrene clusters in supplementary materials. The spectra obtained for neutrals are reported in Fig. 2. Note that the geometries involved in the present work and shown in Figure 3 are the lowest ones found with DFTB global optimization simulations in our previous work [74](or the same consistently relaxed in the DFT/B3LYP approach). They are different from the ones explored by Ricca *et al.* [59]. The dimer and the trimer are stacks presenting twisting, while the tetramer consists of a deformed twisted stack with a side molecule. At both the DFTB and DFT levels, the IR spectra of the neutral clusters are very similar to those of the monomer and the size evolution is hardly visible on the upper plots of Figure 2 showing the full spectrum. The peak modes around 746 and 878 cm^{-1} in DFT are now associated with in-phase out of plane CH bending of the molecules in the stack, while the peak around 3190 cm^{-1} is actually a quite narrow band associated with various CH stretches on the different molecules. The bottom insets of the figure show that the lines in clusters present weak shifts with respect to the monomer lines. With DFT/B3LYP (resp DFTB), the peak maxima of the CH bending modes at 746 (resp 878) cm^{-1} are redshifted by -4 (resp -5) cm^{-1} for the dimer and -6 (resp -7) cm^{-1} for the trimer. This is qualitatively consistent although smaller than the redshifts previously calculated by Ricca *et al.*[59] for the components of those lines in various geometries (in the range -5/-8 cm^{-1} for dimers and -8/-13 cm^{-1} for the trimers) and the redshifts measured experimentally by Roser and Ricca [60]. The DFT peak maximum of the CH stretching band at 3190 cm^{-1} is almost not affected by size ($\pm$ $2cm^{-1}$). The DFTB results are essentially consistent with the DFT results, with spectral shapes very weakly affected by size. Let us mention that the intensity weakness of the mode at 722 cm^{-1} observed for the monomer persists for larger sizes. The 816 cm^{-1} peak is also redshifted up to the trimer, (-4 cm^{-1}), slightly less than the corresponding DFT peak (-7 cm^{-1}) at 878 cm^{-1}. Note however that in the tetramer case, the shift with respect to the monomer is cancelled, certainly due to the hindrance induced by the side molecule. The peak position at 722 cm^{-1} is almost unaffected by size. In contrast, the maximum of the CH stretch band is shifted to the red from 2932 to 2927 cm^{-1}, a trend also observed experimentally [60]. Note that for the two peaks at 746 and 878 cm^{-1} (respectively 722 and 816 cm^{-1} with DFTB), DFT spectra seem to show a monotonic increase of the redshift with the addition of molecules, which is much less stringent at the DFTB level. This could stem from the different dispersion terms or also from the pointwise charge approximation used in the Coulomb contribution. Obviously, the present results must be taken with care because of the inherent approximations of DFTB. They do not include anharmonicity, whose magnitude is also of a few cm^{-1} on the monomer[88], certainly transferable and possibly enhanced in clusters. Finally one can also see that neither in DFT nor in DFTB, the intermolecular modes, associated with low frequencies, have significant intensities in the spectra, certainly because in the neutral species, those modes are characterized by vanishing dipole variations either within the monomers or over the cluster.

The geometries of the cationic clusters, taken from Dontot *et al.*[74], are shown in Figure 3. They are similar however not identical to those of neutral clusters, since the intermolecular twists within the stack are different. The spectra of cationic dimers (Figure 4) present the same main trends as the one of the cationic monomer, characterized by a weak intensity of the CH stretching mode in comparison with the neutrals. Concerning the relative intensities of the bands in the 700-1000 cm^{-1} region versus those in the 1000-2000 cm^{-1} region, the charge effect is even more pronounced in the dimer as compared to that previously reported for the monomer, as the bands in the range 700-1000 cm^{-1} (CH out of plane bending modes) have very weak intensity. It is worth mentioning that these trends are well reproduced at the DFTB level, computed

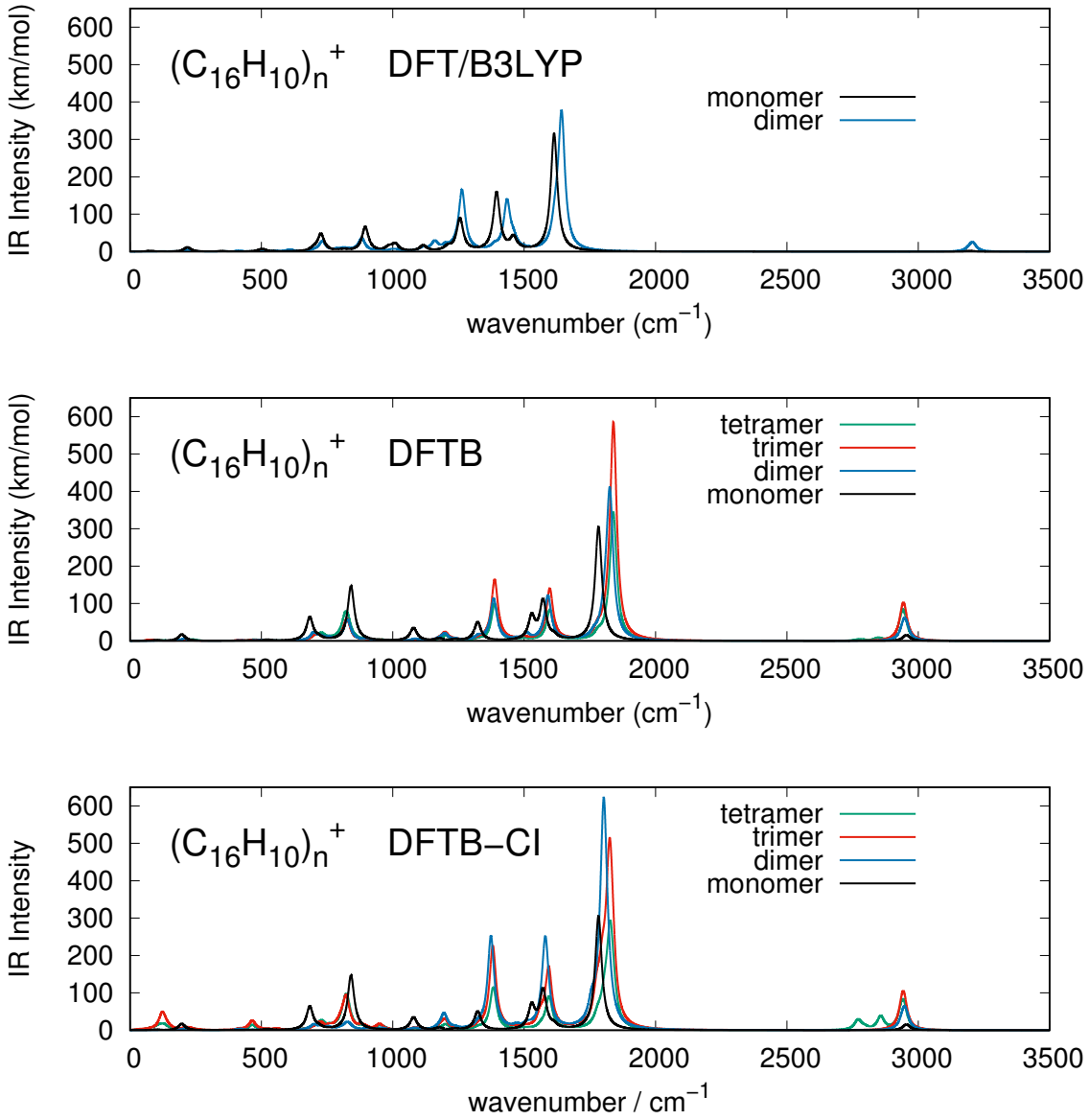

Fig. 4. Harmonic IR spectra of $(C_{16}H_{10})^{+}_{n=1,4}$ clusters from DFT/B3LYP (top), DFTB (medium) and DFTB-CI (bottom) calculations.

with and without the CI scheme. The first observation is that in cationic clusters, oppositely to neutral clusters, size effects have a non negligible influence on the spectra, as can be seen in Figure 4. In the dimer, obviously both the DFTB and DFTB-CI schemes lead to the same charge delocalization pattern, that is an equal sharing of the charge over the two units. The DFT intensities of the maxima at 1395 and 1459 cm^{-1} are inverted, producing a major peak located around 1432 cm^{-1}. The peak located in the monomer around 1613 cm^{-1} is now blueshifted by almost 30 cm^{-1}. The same merging is observed in the dimer with DFTB and DFTB-CI for the lines at 1528 and 1572 cm^{-1} merging into a single peak at 1590 cm^{-1}. The DFTB-CI band at 1781 cm^{-1} is also blueshifted to the region 1801-1826 cm^{-1}. A similar behaviour is observed for the larger sizes n=3 and 4. Let us notice nevertheless that for the trimer and the tetramer, the band intensities in the regions 698-762 and 816-826 cm^{-1} tend to increase, a trend that can probably be attributed to the fact that the charge (expressed in units of electrons) is now shared by several units and its average decreases on each one namely (DFTB-CI values) 0.46/0.27/0.26 in the trimer and 0.49/0.25/0.24/0.02, in the tetramer, the side molecule being almost neutral. When the cluster size increases, the contribution of neutral molecules should tend to increase. Interestingly, this can be observed (Figure 5, right) in the re-emergence for sizes n=3 and 4 of a weak feature around 2945 cm^{-1}, the region of the CH stretch

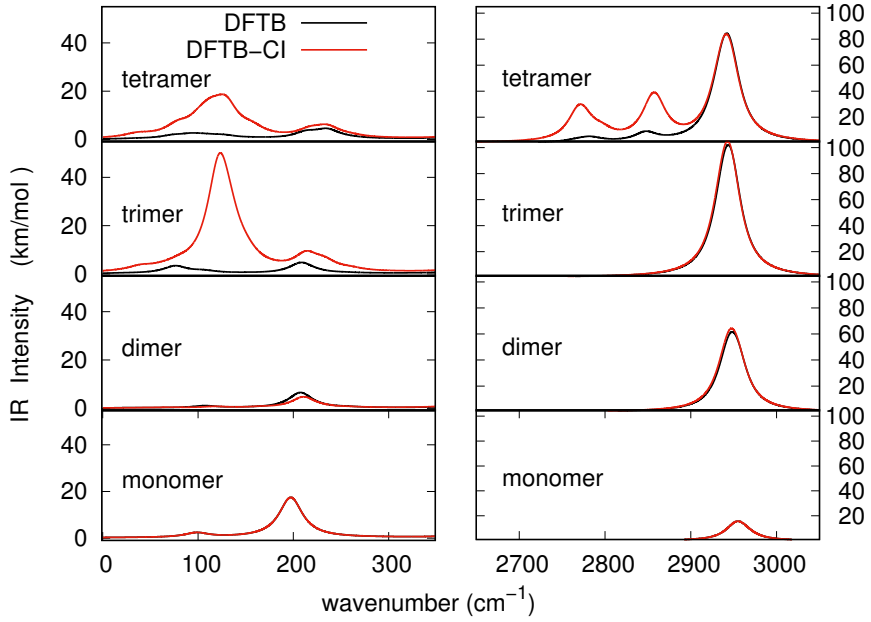

Fig. 5. Zoom views of the harmonic IR spectra of cationic pyrene clusters (n=1-4, from bottom to top) in regions 0-350 cm^{1} (left) and 2700-3100 cm^{-1} (right), comparing DFTB and DFTB-CI calculations.

mode, the most active in the neutral monomer and almost absent in the monomer cation. This feature is further enhanced in DFTB-CI calculation. In the tetramer, one may notice a triplet peak structure in the DFTB-CI spectrum at 2769, 2854 and 2939 cm^{-1}, due to the influence of the side molecule above the stack. Finally, another feature which is specific of the ions concerns the intermolecular modes and the appearance of a weak but visible intensity pattern at very low frequency around 122 cm^{-1} as can be seen in the left panel of Figure 5. In the trimer, a mode at 79 cm^{-1} (DFTB-CI) is associated with a change of the diedral angles between almost internally rigid monomers. The mode at 122 cm^{-1} couples this diedral fluctuation with folding of the monomer carbon skeleton. In the neutrals, those modes had vanishing intensities. In the cation, the small but existing intensities of those modes may reflect charge fluctuations between the various molecules. Similar modes are observed in the tetramer at 79 (diedral) and 129 cm^{-1} (diedral coupled with monomer folding).

At this point, it may be worth to comment about the difference for ions between DFTB and DFTB-CI. A partial relocalization of the charge is observed in DFTB-CI *vs* DFTB, namely 0.46/0.27/0.26 and 0.49/0.25/0.24/0.02 for the trimer and the tetramer respectively instead of 0.35/0.32/0.30 and 0.38/0.30/0.30/0.02 in simple DFTB. This does not considerably affect the cluster spectra. Nevertheless, the account of non-dynamical correlation *vs* mean field charge average and the avoidance of self-interaction in DFTB-CI, especially for extended systems, probably provides a better balance between neutral and ionized monomers. Indeed DFTB-CI explicitly considers the resonance of configurations with the charge based on a single monomers, while simple DFTB (and to some extent DFT, even though hybrid methods avoid a part of self-interaction) intrinsically considers average charges on the monomers, which may not be equivalent in terms of dipole fluctuations. This seems to be responsible for a more pronounced account of the intensity of the very soft modes and of the triplet structure of the CH stretch mode of the tetramer.

We now focus on the distribution of vibrational frequencies. As can be seen in figure 6 (top) for dimers and tetramers, the distribution of these frequencies hardly depends on the cluster charge. The largest discrepancies occurs for the C-H stretching modes around 3000 cm^{-1} and are already present in the monomers. We compare now the computed vibrational frequencies with those resulting from an extrapolation model [75], allowing to address larger sizes. In this approach, one considers that the total number of modes $3nN_{at} - 6$ of a given cationic cluster of size n can be simply separated in $n_{inter} = 6n - 6$ intermolecular modes and $n_{intra} = n(3N_{at} - 6)$ intramolecular modes, where N_{at} is the number of atoms in the pyrene molecules. The intramolecular modes are obtained as the addition of the monomer cation modes $\{\omega_1^+, \omega_2^+, ..., \omega_{72}^+\}$ and those of $n-1$ neutral monomers $(n-1) \times \{\omega_1^0, \omega_2^0, ..., \omega_{72}^0\}$. Intermolecular modes are linearly extrapolated between ω =13 cm^{-1} and the lowest frequency monomer mode :

$$\omega_i = \omega + (\omega_1^+ - \omega)\frac{(i-1)}{n_{inter}}, i = 1, n_{inter} \qquad (2)$$

Despite the crudeness of this model (the charge fluctuation over several molecules is completely neglected, in-

tramolecular modes are considered unperturbed, etc.), a fairly good agreement is obtained when constructing the modes of the dimer and tetramer and comparing them to the actual DFTB-CI calculation, as shown in the difference spectrum (Figure 6, bottom). For the dimer, the frequencies are well reproduced for the cation and the agreement is excellent for the neutral. Of course, the largest the cluster, the minor the contribution of the charge. For the tetramer both neutral and cation frequencies are equally well reproduced. However, a clear departure is observed for some of the high frequency CH modes: this is due to H atoms pointing towards the plane of the side pyrene molecule (see figure 3 for the structure of the tetramer) and such steric effects cannot be reproduced by this additive model. The model can however be applied to arbitrarily large clusters, thus approaching the bulk limit and can be used to determine heat capacities in the harmonic approximation for the frequencies. Figure 7 shows the evolution of the heat capacities from the small cluster cations and up to 2000 molecules. For this largest size, we find a heat capacity in reasonable good agreement with the pyrene bulk experimental one [90], as can be seen in figure 7, except obviously for the peak associated to a phase transition, out of reach by the present additive model. To some extent, this agreement of an intensive observable is somewhat consistent with the reasonable reliability of the present DFTB monomer vibrational structure discussed above despite the various approximations inherent to DFTB and the harmonic approximations.

4 Conclusion

We have reported a comparison of normal mode analysis for pyrene clusters containing up to 4 units, involving DFT, DFTB and DFTB-CI in the full range spectrum up to $\approx$ 3300 cm^{-1}. In the case of neutrals, little change is observed with size, both at the DFT and DFTB levels. The present DFTB IR spectra are generally consistent with the DFT/B3LYP ones and also with the previous results of Ricca *et al.*[59], even though quantitative shifts of a few cm^{-1} are quite delicate to estimate accurately, whatever the above methods. The situation of the pyrene cation clusters is significantly different from that of neutrals and essentially follows that of the cation monomer up to size n=4. The spectra show a strong attenuation of the CH stretch band around 3000 cm^{-1} and a strong reduction of the intensity between 700-1000 cm^{-1}, the region of the out of plane CH bending. The bands in the 1000-2000 cm^{-1} spectral range conserve their strong intensity from the cationic monomer to the tetramer. However, the CH stretch modes recover some perceptible intensity when the number of units increases. Another noticeable feature is that, while the intermolecular modes have almost no intensity in the neutrals, diedral fluctuation modes within the trimer stacks become somewhat active in the cationic clusters, possibly coupled with monomer folding motion.

Obviously, the question may arise about the challenge and ability of DFTB and DFTB-CI to address such small vibrational shifts induced by size or the transferability to different species. Indeed, while the qualitative change in the spectra due to charge are correctly accounted for as shown in the above results for the monomer, some absolute frequencies show errors of the order of 100-200 cm^{-1}. However, it was shown in a number of previous studies dealing with IR spectroscopy (harmonic and also including anharmonicities from molecular dynamics simulation) of various systems that spectral shifts are well accounted for, despite the discrepancies in the absolute line positions. This includes cases with significant spectral changes (varying the charge and/or the PAH size) as well as delicate shifts due to perturbations induced by clustering[91,81,92,93], chemical attachment[94,81] or matrix environment[95,96]. In neutral molecular clusters, clearly the bonding relies on a phenomenological dispersion contribution in DFTB (+D) or in DFT(+D3) and the present results seem to be reasonably consistent with the previous DFTB+D3 publication[59], despite the differences in the equilibrium structures. Thus it seems likely that the trends determined in the present work are correct and possibly transferable to other molecular clusters of the PAH family with larger units and/or larger sizes and possibly complexes, even though higher level calculations such as Coupled Cluster carried out in sufficiently large basis sets, nowadays out of reach with sufficiently extensive basis sets, are certainly desirable.

We hope that the present study brings some new insight in the spectroscopy of PAH-containing compounds and possibly help for the detection of PAH clusters or small grains in interstellar or circumstellar media. A perspective of the present work would be to investigate the anharmonic effects via molecular dynamics simulations which is possible either with DFTB or DFTB-CI and also potentially to explore the evolution of the IR spectra with temperature.

5 Acknowledgements

The authors thank the CALMIP HPC center for computational support. L. D. acknowledges ERC for support under grant ERC-2013- Syg-610256-NANOCOSMOS and EUR grant NanoX n 080876 in the framework of the "Programme des Investissements d'Avenir".

Author contribution L.D. performed the IR spectra calculations. S.Z. developed the frequency interpolation model. M.R. developed the extensions of DFTB used to compute IR spectra. F.S. made the pictures. All authors participated to the scientific discussions and writing of the paper.

References

1. N. A. Eaves, S. B. Dworkin, M. J. Thomson, Proc. Comb. Inst., **35**, 1787 (2015)
2. A. Violi, S. Izvekov, Proc. Comb. Inst., **31**, 529 (2007)
3. A. D'Anna, M. Sirignano, J. Kent, Combust. Flame, **157**, 2106 (2010)

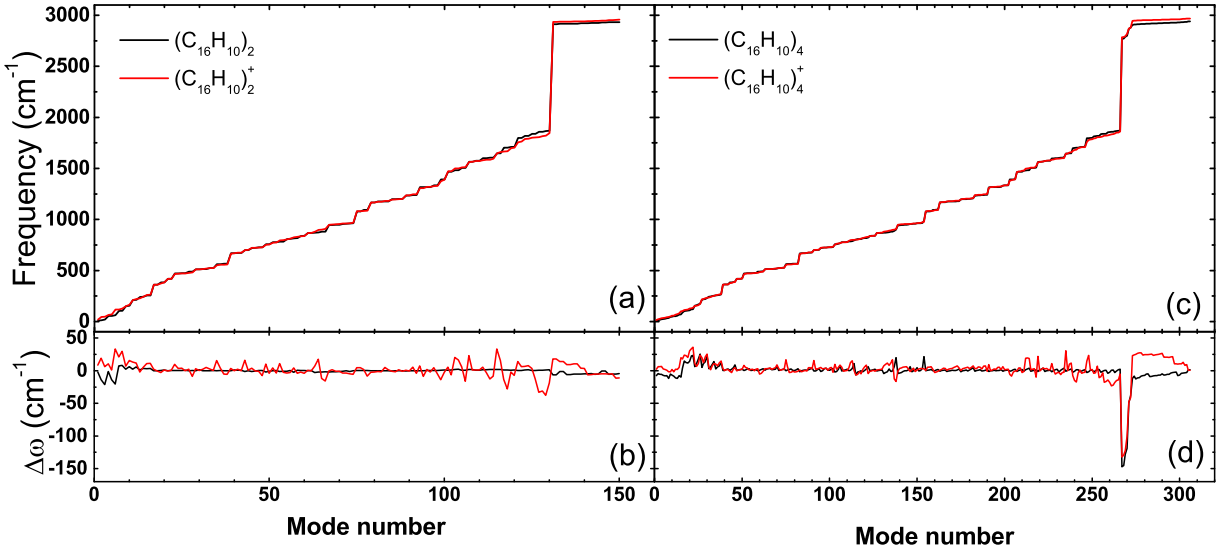

Fig. 6. Harmonic frequencies computed at the DFTB-CI level for neutral and cationic dimers (a) and tetramers (c). Differences between frequencies at the DFTB-CI level and from the extrapolation model for the dimer (b) and the tetramer (d) (see text).

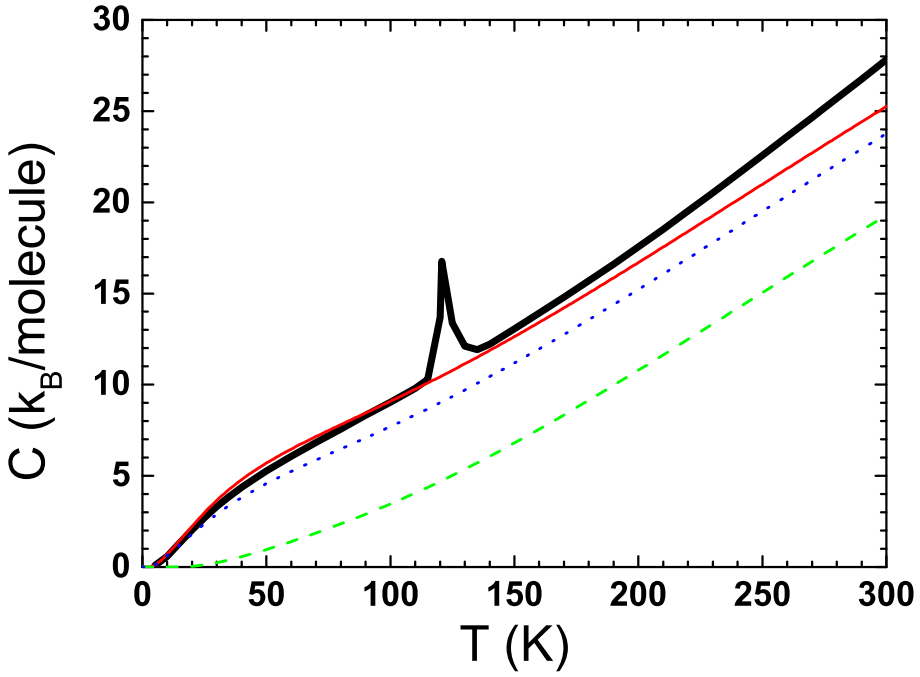

Fig. 7. Comparison of the bulk heat capacity (black line) [90] to the calculated ones using the extrapolation model for the vibration modes described in the text, for: the monomer (green dashed line), the tetramer (blue point line) and a cluster of 2000 pyrene molecules (red line).

4. T. S. Totton, A. J. Misquitta, M. Kraft, Phys. Chem. Chem. Phys., **14**, 4081 (2012)
5. A. Raj, M. Sander, V. Janardhanan, et al., Combust. Flame, **157**, 523 (2010)
6. Q. Mao, A. C. T. van Duin, K. H. Luo, Carbon, **121**, 380 (2017)
7. C. Saggese, S. Ferrario, J. Camacho, et al., Combust. Flame, **162**, 3356 (2015)
8. D. Aubagnac-Karkar, A. El Bakali, P. Desgroux, Combust. Flame, **189**, 190 (2018)
9. T. S. Totton, D. Chakrabarti, A. J. Misquitta, et al., Combust. Flame, **157**, 909 (2010)
10. C. S. Wang, N. C. Bartelt, R. Ragan, et al., Carbon, **129**, 537 (2018)
11. H. Sabbah, L. Biennier, S. J. Klippenstein, et al., J. Phys. Chem. Lett., **1**, 2962 (2010)
12. E. M. Adkins, J. A. Giaccai, J. H. Miller, Proc. Comb. Inst., **36**, 957 (2017)
13. T. Heinemann, K. Palczynski, J. Dzubiella, et al., J. Chem. Phys., **143**, 174110 (2015)
14. P. Grančič, R. Bylsma, H. Meekes, et al., Crystal Growth & Design, **15**, 1625 (2015)
15. I. Fedorov, Y. Zhuravlev, V. Berveno, Phys. Stat. Sol.(b), **249**, 1438 (2012)
16. S. E. Fioressi, R. C. Binning, D. E. Bacelo, Chem. Phys. Lett., **454**, 269 (2008)
17. J. C. Sancho-García, A. J. Pérez-Jiménez, The Journal of Chemical Physics, **141**, 134708 (2014)
18. Y. Yoshida, K. Isomura, H. Kishida, et al., Chemistry – A European Journal, **22**, 6023 (2016)
19. S. Sanyal, A. K. Manna, S. K. Pati, J. Phys. Chem.C, **117**, 825 (2013)
20. R. Scholz, R. Luschtinetz, G. Seifert, et al., J. Phys. Condens. Matter, **25**, 473201 (2013)
21. A. A. M. H. M. Darghouth, M. E. Casida, W. Taouali, et al., Computation (2015)
22. S. O. Baek, R. a. Field, M. E. Goldstone, et al., Water Air Soil Pollut, **60**, 279 (1991)
23. C.-T. Li, H.-K. Zhuang, L.-T. Hsieh, et al., Environ. Int., **27**, 61 (2001)
24. M. Blanchard, M.-J. Teil, E. Guigon, et al., Sci. Total Environ., **375**, 232 (2007)
25. A. Birgül, Y. Tasdemir, S. S. Cindoruk, Atmos. Res., **101**, 341 (2011)
26. A. D. P. Netto, T. M. Krauss, I. F. Cunha, et al., Water Air Soil Pollut, **176**, 57 (2006)
27. A. Léger, J. L. Puget, Astron. Astrophys., **137**, L5 (1984)
28. L. J. Allamandola, A. G. G. M. Tielens, J. R. Barker, Astrophys. J. Lett., **290**, L25 (1985)
29. G. P. van der Zwet, L. J. Allamandola, Astron. Astrophys., **146**, 76 (1985)
30. A. Leger, L. D'Hendecourt, Astron. Astrophys., **146**, 81 (1985)
31. M. K. Crawford, A. G. G. M. Tielens, L. J. Allamandola, Astrophys. J. Lett., **293**, L45 (1985)
32. F. Salama, E. L. O. Bakes, L. J. Allamandola, et al., Astrophys. J. , **458**, 621 (1996)
33. M. Rapacioli, C. Joblin, P. Boissel, Astron. Astrophys., **429**, 193 (2005)
34. O. Berné, C. Joblin, Y. Deville, et al., Astron. Astrophys., **469**, 575 (2007)
35. O. Berné, C. Joblin, M. Rapacioli, et al., Astron. Astrophys., **479**, L41 (2008)
36. Y. M. Rhee, T. J. Lee, M. S. Gudipati, et al., Proc. Natl. Acad. Sci. Unit. States Am., **104**, 5274 (2007)
37. A. K. Lemmens, S. Gruet, A. L. Steber, et al., Phys. Chem. Chem. Phys., **21**, 3414 (2019)
38. T. Chen, Astrophys. J. , **866**, 113 (2018)
39. J. Zhen, T. Chen, A. G. G. M. Tielens, The Astrophysical Journal, **863**, 128 (2018)
40. S. R. Langhoff, The Journal of Physical Chemistry, **100**, 2819 (1996)
41. M. Vala, J. Szczepanski, F. Pauzat, et al., The Journal of Physical Chemistry, **98**, 9187 (1994)
42. C. W. Bauschlicher, S. R. Langhoff, Spectrochimica Acta Part A: Molecular and Biomolecular Spectroscopy, **53**, 1225 (1997)
43. C. W. Bauschlicher, Jr., Astrophys. J., **564**, 782 (2002)
44. M. Bahou, Y.-J. Wu, Y.-P. Lee, The Journal of Physical Chemistry Letters, **4**, 1989 (2013)
45. F. Calvo, M. Basire, P. Parneix, The Journal of Physical Chemistry A, **115**, 8845 (2011)
46. C.-H. Chin, S. H. Lin, Physical Chemistry Chemical Physics, **18**, 14569 (2016)
47. I. Garkusha, J. Fulara, J. P. Maier, Journal of Molecular Structure, **1025**, 147 (2012)
48. F. X. Hardy, O. Gause, C. A. Rice, et al., Astrophys. J. Lett., **778**, L30 (2013)
49. M. Rapacioli, F. Calvo, F. Spiegelman, et al., J. Phys. Chem.A, **109**, 2487 (2005)
50. M. Rapacioli, F. Spiegelman, D. Talbi, et al., J. Chem. Phys., **130**, 244304 (2009)
51. Y. Zhao, D. G. Truhlar, J. Phys. Chem.C, **112**, 4061 (2008)
52. J. Hernández-Rojas, F. Calvo, D. J. Wales, Phys. Chem. Chem. Phys., **18**, 13736 (2016)
53. R. Podeszwa, J. Chem. Phys., **132**, 044704 (2010)
54. M. Bartolomei, F. Pirani, J. M. C. Marques, J. Phys. Chem.C, **121**, 14330 (2017)
55. O. I. Obolensky, V. V. Semenikhina, A. V. Solov'yov, et al., Int. J. Quant. Chem., **107**, 1335 (2007)
56. J. Hernández-Rojas, F. Calvo, S. Niblett, et al., Phys. Chem. Chem. Phys., **19**, 1884 (2017)
57. J. D. Herdman, J. H. Miller, J. Phys. Chem.A, **112**, 6249 (2008)
58. L. Pascazio, M. Sirignano, A. D'Anna, Combust. Flame, **185**, 53 (2017)
59. A. Ricca, J. Charles W. Bauschlicher, L. J. Allamandola, Astrophys. J. , **776**, 31 (2013)
60. J. E. Roser, A. Ricca, Astrophys. J. , **801**, 108 (2015)
61. M. Rapacioli, F. Calvo, C. Joblin, et al., The Journal of Physical Chemistry A, **111**, 2999 (2007)
62. J. Gräfenstein, E. Kraka, D. Cremer, J. Chem. Phys., **120**, 524 (2004)
63. A. Savin, Recent developments and applications of modern Density Functional Theory, J. Seminario, Elsevier, Amsterdam (1996, p 327–357)
64. T. Leininger, H. Stoll, H.-J. Werner, et al., Chem. Phys. Lett., **275**, 151 (1997)
65. E. Goll, H.-J. Werner, H. Stoll, Phys. Chem. Chem. Phys., **7**, 3917 (2005)
66. J. Toulouse, F. Colonna, A. Savin, Phys. Rev. A, **70** (2004)
67. V. Lutsker, B. Aradi, T. A. Niehaus, J. Chem. Phys., **143**, 184107 (2015)
68. D. Porezag, T. Frauenheim, T. Köhler, et al., Phys. Rev.B, **51**, 12947 (1995)

69. G. Seifert, D. Porezag, T. Frauenheim, Int. J. Quantum Chem., **58**, 185 (1996)
70. M. Elstner, D. Porezag, G. Jungnickel, et al., Phys. Rev.B, **58**, 7260 (1998)
71. F. Spiegelman, N. Tarrat, J. Cuny, et al., Adv. Phys. X, in press (2020)
72. M. Rapacioli, F. Spiegelman, A. Scemama, et al., J. Chem. Theor. Comput., **7**, 44 (2011)
73. Q. Wu, C.-L. Cheng, T. Van Voorhis, J. Chem. Phys., **127**, 164119 (2007)
74. L. Dontot, F. Spiegelman, M. Rapacioli, The Journal of Physical Chemistry A, **123**, 9531 (2019)
75. S. Zamith, M.-C. Ji, J.-M. L'Hermite, et al., The Journal of Chemical Physics, **151**, 194303 (2019)
76. C. Joblin, L. Dontot, G. A. Garcia, et al., J. Phys. Chem. Lett., **8**, 3697 (2017)
77. M. J. Frisch, et. al., Gaussian 03 Revision A.1 (2016), gaussian Inc. Wallingford CT
78. J. Frenzel, A. F. Oliveira, N. Jardillier, et al., Semi-relativistic, self-consistent charge Slater-Koster tables for density-functional based tight-binding (DFTB) for materials science simulations, TU Dresden (2004-2009)
79. A. Simon, M. Rapacioli, E. Michoulier, et al., Molecular Simulation, **45**, 249 (2019)
80. E. Michoulier, N. Ben Amor, M. Rapacioli, et al., Physical Chemistry Chemical Physics, **20**, 11941 (2018)
81. B. Joalland, M. Rapacioli, A. Simon, et al., J. Phys. Chem.A, **114**, 5846 (2010)
82. T. Heine, M. Rapacioli, S. Patchkovskii, et al., deMon-Nano Experiment 2009, http://physics.jacobs-university.de/theine/research/deMon/
83. C. Joblin, L. D'Hendecourt, A. Leger, et al., Astron. Astrophys., **281**, 923 (1994)
84. D. J. Cook, S. Schlemmer, N. Balucani, et al., The Journal of Physical Chemistry A, **102**, 1465 (1998)
85. H. Kim, D. Wagner, R. Saykally, Physical review letters, **86**, 5691 (2001)
86. E. Maltseva, A. Petrignani, A. Candian, et al., The Astrophysical Journal, **814**, 23 (2015)
87. C. J. Mackie, A. Candian, X. Huang, et al., The Journal of Chemical Physics, **145**, 084313 (2016)
88. G. Mulas, C. Falvo, P. Cassam-Chenaï, et al., The Journal of Chemical Physics, **149**, 144102 (2018)
89. H. Torii, Y. Ueno, A. Sakamoto, et al., The Journal of Physical Chemistry A, **103**, 5557 (1999)
90. W.-K. Wong, E. F. Westrum, The Journal of Chemical Thermodynamics, **3**, 105 (1971)
91. A. Simon, M. Rapacioli, M. Lanza, et al., Phys. Chem. Chem. Phys., **13**, 3359 (2011)
92. A. Simon, C. Joblin, N. Polfer, et al., J. Phys. Chem.A, **112**, 8551 (2008)
93. A. Simon, M. Rapacioli, J. Mascetti, et al., Physical Chemistry Chemical Physics, **14**, 6771 (2012)
94. B. Joalland, A. Simon, C. J. Marsden, et al., Astron. Astrophys., **494**, 969 (2009)
95. C. Iftner, A. Simon, K. Korchagina, et al., J. Chem. Phys., **140**, 034301 (2014)
96. A. Simon, C. Iftner, J. Mascetti, et al., J. Phys. Chem. A, **119**, 2449 (2015)